Two-dimensional interferometric and synthetic aperture imaging with a hybrid terahertz/millimeter wave system

Ke Su,[1,*] Zhiwei Liu,[1] Robert B. Barat,[2] Dale E. Gary,[1] Zoi-Heleni Michalopoulou,[3] and John F. Federici[1]

[1]Department of Physics, New Jersey Institute of Technology, Newark, New Jersey 07102, USA

[2]Otto York Department of Chemical Engineering, New Jersey Institute of Technology, Newark, New Jersey 07102, USA

[3]Department of Mathematical Sciences, New Jersey Institute of Technology, Newark, New Jersey 07102, USA

*Corresponding author: ks265@njit.edu

Received 11 December 2009; accepted 4 March 2010;
posted 23 March 2010 (Doc. ID 121332); published 7 April 2010

We have developed an interferometric synthetic aperture incoherent imaging system at 94 GHz, in which a high-power electronic millimeter wave source (Gunn Oscillator) is integrated with a continuous-wave terahertz (THz) photomixing detection system to achieve a high signal-to-noise ratio. Imaging of a point source located 10 m away from the detector array is presented. Two-dimensional THz reflective images of an extended object with different shapes are reconstructed with only four detectors by use of rotational synthesis.

OCIS codes: 110.6795, 110.3175.

1. Introduction

Recently, terahertz (THz) imaging has attracted increased attention because of its application in security screening, medicine, and stand-off detection of explosives [1,2]. Various techniques for THz imaging have been reviewed by Chan *et al.* [3]. The most popular THz imaging method, first demonstrated by Hu and Nuss [4], uses THz pulsed time-domain spectroscopy (TDS). Using this method, two-dimensional (2-D) images are acquired on a pixel-by-pixel basis. Two-dimensional electro-optic imaging using continuous-wave (cw) radiation was reported by Wu *et al.* [5]. For this imaging method, THz radiation is generated by beating or mixing two near-infrared laser sources in a THz photomixer. The output THz frequency is given by the difference frequency between the two infrared sources. One of the limitations in applying either the THz TDS or cw photomixing systems to imaging is the requirement for phase coherency between the optical sources that both generate and detect THz radiation.

Over the past few years, a new method of THz imaging, called THz synthetic aperture imaging, has emerged. Synthetic aperture imaging methods are usually used in astronomy and radar ranging [6]. These methods utilize the THz phase and amplitude measured from multiple positions to reconstruct a THz image. Synthetic aperture THz impulse imaging, which is similar to optical holography, has been demonstrated by McClatchey *et al.* [7]. For this imaging method, a target is illuminated with pulsed THz, and a gated THz receiver records the scattered field. A frequency dependent amplitude and phase can then be extracted to reconstruct the geometric shape of the target. Some methods have been developed to solve the inverse problem of image reconstruction by numerically backpropagating measured scattered THz transients [8,9]. O'Hara and Grischkowsky [10–12] developed synthetic phased array THz imaging methods that utilize arrayed optical

0003-6935/10/190E13-07$15.00/0

mirrors to reconstruct field amplitude or energy density, diffraction-limited THz images. Recently, Löffler and his group [13,14] developed a hybrid system that combines a high-power electronic THz source with a Ti:sapphire pulsed laser. Based on heterodyne detection, a 2-D reflected-amplitude image can be generated through a raster scan by moving the object by means of an $x-y$ translation stage.

Rather than using a single detector and multiple mirror orientations as in the synthetic phased array approach or using two detectors based on raster-scan imaging, interferometric synthetic aperture imaging detects the THz electric field at multiple locations and then uses the correlated phase and amplitude of the electric field from various pairs of detectors to reconstruct the image. The synthetic aperture imaging method described here does not require the source to be phase coherent with the detector. Consequently, there is some flexibility in integrating a high power source with an independent detection array. In our previous study, we simulated THz interferometric images [15] and demonstrated one-dimensional imaging of a THz point source [16] and near-field correction of incoming THz wavefronts [17]. We expanded the technique and demonstrated 2-D THz images using only one THz detector placed at N positions to simulate the performance of an N-element detector array [18]. Recently, we achieved video-rate interferometric imaging of a point source using an array of four detectors [19] in which the imaging rate reached 62 frames/s. In the previous study [18,19], the same lasers that power the THz generation were also used for the detection process. Consequently, cw generation and detection of THz radiation was phase coherent.

Unlike the THz imaging system described in [18,19], the system described here does not require cw generation and detection of radiation to be phase coherent. Based on heterodyne detection, we configured a hybrid THz/millimeter wave system that integrates a relatively high power electronic millimeter wave source (Gunn Oscillator), which is just below the THz spectral range, into the cw THz photomixing detection system. There is sufficient sensitivity in the THz receivers to detect radiation at 94 GHz. This imaging system is capable of imaging a source at a distance of more than 10 m, thereby illustrating the potential of interferometric imaging for stand-off detection when high power THz sources are available. In addition to improved stand-off imaging distances, the high power source enables the demonstration of 2-D interferometric imaging of an extended object. By analyzing the amplitude and phase signals for different pairs of detectors and performing the correlation of each baseline, we can successfully reconstruct 2-D images of an extended object with different shapes.

2. Terahertz Interferometric Synthetic Imaging Method and Detector Array Configuration

The detailed THz interferometric synthetic imaging theory was presented earlier [15–19]. Here, we show only the main formulas of this method; the dependence of image quality on the U–V data distribution is discussed. In synthetic aperture imaging, the THz electric field is detected simultaneously at multiple locations using an array of individual THz detectors. A correlation of the electric field is calculated for each pair of detectors in the array. Each correlation provides one spatial Fourier component in the Fourier transform (U–V) plane that contains the target information. Finally the image of the target is reconstructed through Fourier inversion using the U–V data of all the different detector pair combinations. Higher image quality can be achieved through a larger number of U–V points. Unlike a focal plane array, geometry in which the detectors are evenly spaced in the interferometric array, it is better to space the receivers in an aperiodic arrangement, leading to more complete coverage of the U–V plane and, consequently, more nonredundant Fourier components in the reconstructed images.

The 2-D image is generated through Fourier inversion:

$$\sigma_E(\xi,\eta) = \sum_{l=1}^{N(N-1)/2} [\mathrm{Re}(A_l e^{i\Delta\phi_l}) \cos(k(\mu_l\xi + v_l\eta)) - \mathrm{Im}(A_l e^{i\Delta\phi_l}) \sin(k(\mu_l\xi + v_l\eta))], \quad (1)$$

where N is the number of the detectors. There are $N(N+1)/2$ pairs of detectors to be correlated, which corresponds to $N(N+1)/2$ U–V points in the Fourier transform plane. μ_l and v_l are baseline components between the detector pair m and n, which can be expressed as differences of coordinates: $\mu_l = (x_n - x_m)$ and $v_l = (y_n - y_m)$. A_l and $\Delta\phi_l$ are the correlated amplitude and phase of detector pair m and n, which can be expressed as $A_l = E_m E_n$ and $\Delta\phi_l = \phi_m - \phi_n$, respectively. $\xi = x'/Z_0$ and $\eta = y'/Z_0$ are the angular coordinates for point (x', y') on the source surface. Z_0 is the distance between the source and the detector array.

The angular resolution of a planar array can be approximately expressed as

$$\theta = \frac{\lambda}{b}, \quad (2)$$

where b is the baseline length of the imaging array and λ is the THz wavelength. At a distance Z_0 away, the lateral spatial resolution is

$$\Delta L_{\mathrm{lat}} = \theta \cdot Z_0 = \frac{\lambda \cdot Z_0}{b}. \quad (3)$$

In our current experiment, only four THz receivers are used. Figure 1(a) shows the geometric arrangement of four receivers ($N = 4$) at Cartesian coordinates $(-38.7\,\mathrm{mm}, 0)$, $(0, -29.27\,\mathrm{mm})$, $(32.4\,\mathrm{mm}, 0)$, and $(0, 35.5\,\mathrm{mm})$. Figures 1(b) and 1(c) show the corresponding U–V distribution. Components u and v are spatial frequencies that can be expressed as the spatial distance in wavelength units

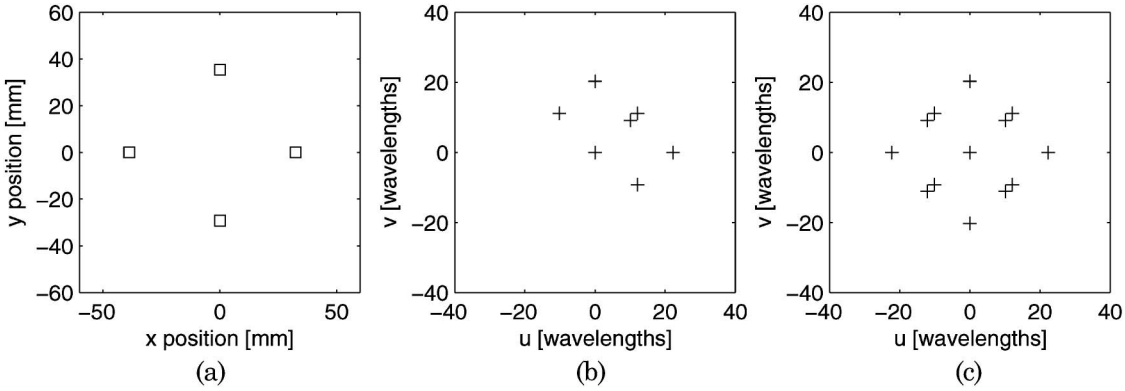

Fig. 1. (a) Four detector array, (b) corresponding distribution of points in the U–V plane , (c) U–V point distribution with symmetry.

$$\left(u = \frac{x_n - x_m}{\lambda}, v = \frac{y_n - y_m}{\lambda}\right).$$

There are $N(N+1)/2 = 6$ unique baselines [shown in Fig. 1(b)], but there are twice this many points that are due to symmetry [shown in Fig. 1(c)].

Using this geometric arrangement, we obtain the image of a point source at various distances. Because of the limitation of coverage of the U–V plane, the array responds optimally only to a specific range of spatial scales. More complete U–V coverage is required for a wider range of shapes. Efficient U–V plane coverage with four detectors can be achieved by rotating the detector array. Figure 2 shows the row geometric arrangement of four individual detectors at Cartesian coordinates $(-56\,\text{mm}, 0)$, $(-27\,\text{mm}, 0)$, $(28\,\text{mm}, 0)$, and $(42\,\text{mm}, 0)$ and the corresponding distribution of U–V points before rotation.

After rotating around the receiver center at 10 deg intervals up to 170 deg, the equivalent number of baselines will increase from 6 to 108, which will dramatically improve the quality of the image. Figure 3(a) shows the equivalent detector arrangement; Fig. 3(b) shows U–V sampling accumulation after 18 rotations.

3. Experimental Results

A. Experimental Setup

The experimental setup for the hybrid cw interferometric imaging system is sketched in Fig. 4. The radiation source is a mechanically tuned Gunn Oscillator (GDM, Millitech, Northampton, Massachusetts) followed by a power amplifier (AMP, Millitech) with 8.5 dB gain. The source consists of a 94 GHz Gunn Oscillator with an output power of 50 mW. After amplification, the radiation is launched by a horn antenna with an output power of 354 mW. The cw 94 GHz radiation is detected by photomixing at the beat frequency of two distributed feedback (DFB) diode lasers (DLs) (DC110, TOPTICA Photonics, Munich, Germany) operating near 852 nm. In this experiment, the DFB lasers are detuned by 94 GHz to match the source. The output of the DFB lasers is evenly split by the first pair of beam splitters and then combined using the second pair of beam splitters. The combined beam is coupled into polarization-maintaining optical fibers using FiberPort collimators (PAF-X-5-A, Thorlabs, Newton, New Jersey) and finally delivered into four THz receivers. The receivers are low-temperature grown GaAs bowtie-type photoconductive dipole antennas (PDAs). Approximately 20 mW of optic power is used to excite the THz receiver. A bias of ± 12 V DC is applied to power the receiver electronics.

Note that there is no adjustable phase or path length delay in the cw opto-electronic THz detection hardware. The GDM source is phase incoherent with respect to the receiver. Moreover, there is no active frequency locking of the GDM source to the beat frequency of the DFB lasers. Our previous demonstration of 2-D interferometric imaging [19] utilized a

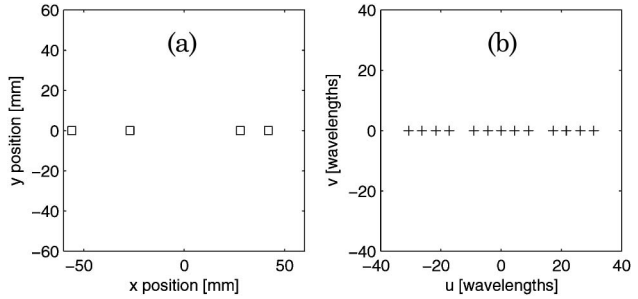

Fig. 2. (a) Four detector array with row configuration and (b) corresponding distribution of points in the U–V plane.

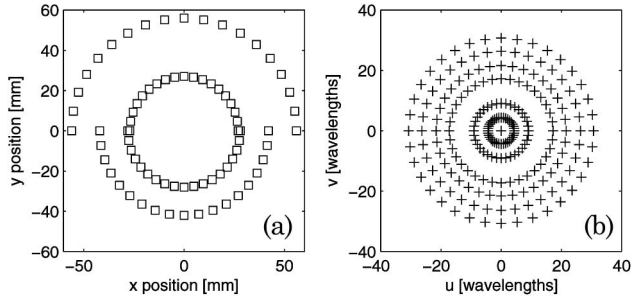

Fig. 3. (a) Four detector array configuration after rotation and (b) corresponding distribution of points in the U–V plane.

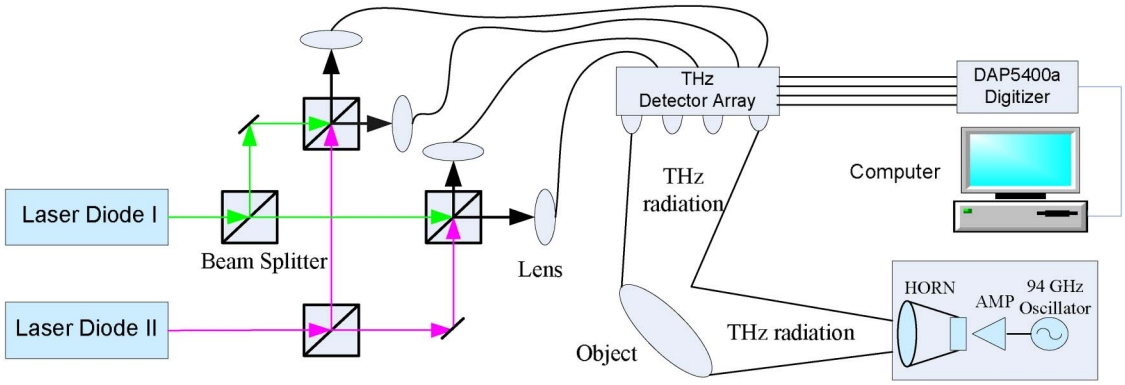

Fig. 4. (Color online) Schematic diagram of the incoherent detection THz interferometric imaging system configuration.

phase coherent PDA THz transmitter rather than an electronic high power source.

The high output power of the source dramatically improves the signal-to-noise ratio (SNR) in comparison with our previous results. An object is illuminated by the 94 GHz radiation with a portion of that radiation reflected toward THz detector array. To increase the number of baselines, the object is mounted on a computer-controlled rotation stage and rotated around the origin point in 10 deg intervals up to 170 deg to simulate the rotation of the detector array. For practical reasons, we rotated the object instead of the detector array: it is difficult to rotate the array while maintaining fixed relative positions of the detectors since the individual detectors are sensitive to the polarization of the incoming THz radiation. We used a multichannel digitizer (DAP5400a, Microstar Laboratories, Bellevue, Washington) to collect the data from four detectors simultaneously. The digitizer acquired 14 bit data at 256 Ksamples/s on each of four channels. The sampling rate is set to 128 kHz. The amplitude and phase information of each individual receiver before correlation was obtained by fast Fourier transform onboard digital signal processing capability.

B. Stand-Off Detection of the Image of the Terahertz Source

To detect a THz signal, the beat frequency of two DFB lasers should match the frequency of the source (0.094 THz). The source bandwidth is ~20 MHz, and the electronic bandwidth of the THz PDA receiver is approximately 1 MHz. The 1 MHz electronic bandwidth corresponds to the intermediate frequency (IF) bandwidth of the optical heterodyne THz PDA receiver. For our experiments, the frequency of the source is fixed while we vary the difference frequency of the DFB lasers to tune the cw photomixing receiver to 94 GHz. As the detection array is tuned closer to the frequency of the source, the detected signal from the PDA within the 1 MHz detection bandwidth increases. Figure 5(a) shows the IF spectrum of the 1 MHz bandwidth the PDA receiver captured with a digital spectrum analyzer. Different lines correspond to various frequency detunings of the detected THz frequency relative to the frequency of the source. As the beat frequency of the two lasers approaches the frequency of the source, the detected signal in the 1 MHz bandwidth increases. The lasers are tuned to maximize this signal amplitude. For reconstruction of the image, the output of each detector is digitized. A sample Fourier transform of the digitized waveform from one detector is shown in Fig. 5(b). The top line corresponds to tuning the source and the cw photomixing array to a maximum signal and the bottom line corresponds to a large (>20 MHz) detuning of the source and detection frequency.

The previous THz video-rate imaging system described in [19] used a phase modulator that operated at 100 kHz, which was inserted into the optical path. To reconstruct the video-rate images, only the point at 100 kHz in the sample spectrum was collected to obtain the amplitude and phase information. However, the imaging system described in this paper does not require a phase modulator. With the sampling rate at 128 kHz, the whole band signal (including phase and amplitude) is integrated and then averaged over the whole bandwidth of the detector to perform image reconstruction. This signal processing dramatically improves the stability of the correlation phase of the baseline and hence the stability of the reconstructed image in comparison with our previous results [19].

From Fig. 5 we can see that the SNR has increased from 12.4 dB [Fig. 5(c)] as acquired from our previous coherent detection system [19] to 45.7 dB [Fig. 5(b)] due to the integration of a high power source with the cw photomixing system. The high SNR improves the stand-off distance for imaging. We demonstrated stand-off imaging distances of 10.3 m with this apparatus. The imaging distance is currently limited by the available laboratory space. Figure 6 shows the comparison of the experimental reconstructed images of the GDM source (top row) at various distances (10.3, 7.4, and 1 m) with the corresponding simulation results (bottom row). Only four receivers with a spiral configuration (refer to Fig. 1) are used to reconstruct images of the pointlike source. The image also shows a periodic pattern or sidelobes that are due to the small number of baselines. The reconstructed experimental images and sidelobe distribution are in good

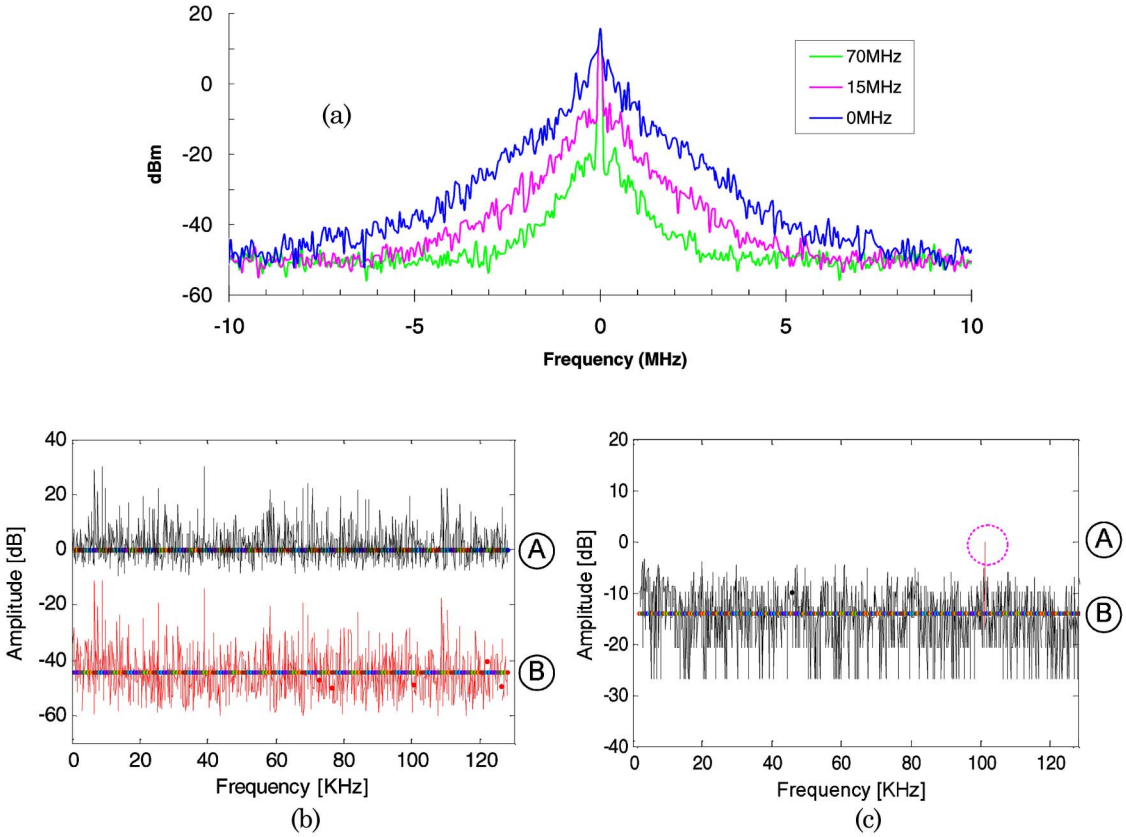

Fig. 5. (Color online) (a) Spectrum of the PDA receiver with 1 MHz bandwidth at detuning frequencies of 70, 15, and 0 MHz. (b) Frequency spectrum of an incoherent detection waveform acquired from the digitizer: A, signal level and B, average noise floor. (c) Frequency spectrum of coherent detection waveform acquired from the digitizer: A, the peak corresponding to the modulation frequency of 100 kHz and B, average noise floor.

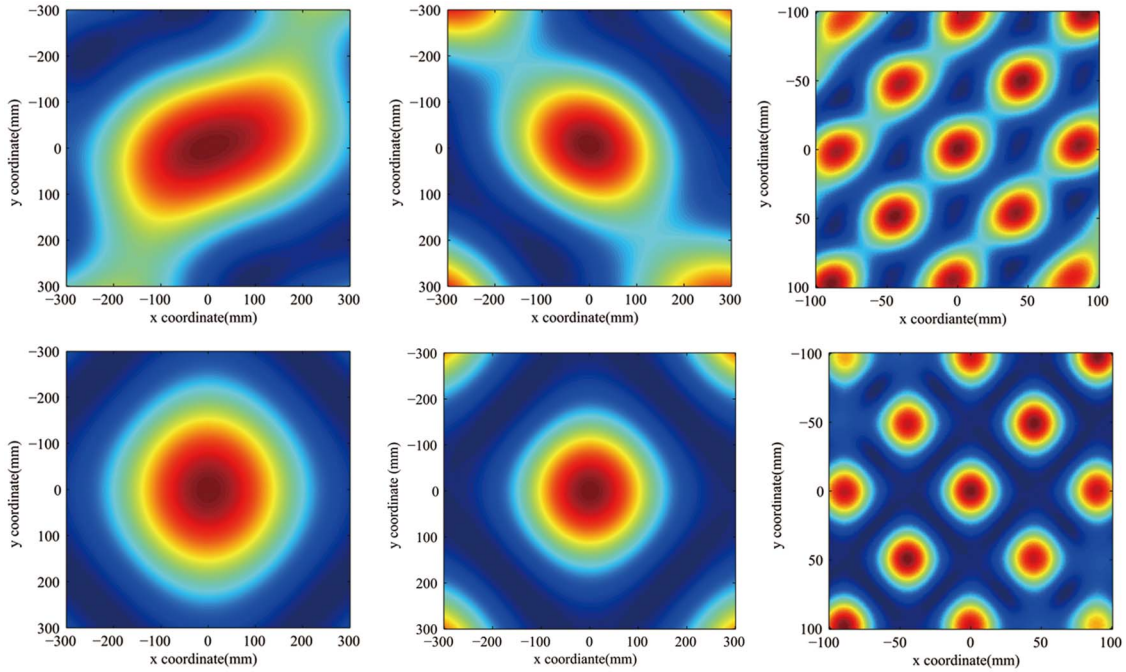

Fig. 6. (Color online) Comparison of THz imaging of the GDM source (top row) and simulations (bottom row) at distances of 10.3 m (left), 7.6 m (middle), and 1 m (right).

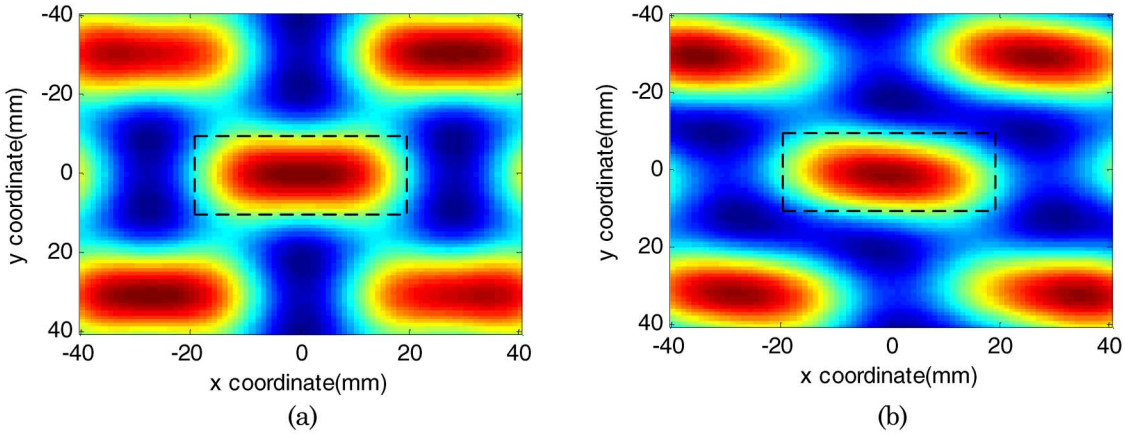

Fig. 7. (Color online) (a) Simulation image of 20 mm by 40 mm rectangles with limited U–V data and (b) THz image reconstructed with the experimental data.

agreement with the simulation. Note that, as the distance between the source and the imaging array increases, the apparent width of the point source increases since the angular resolution of the imaging array [Eqs. (2) and (3)] remains fixed. To achieve longer imaging distances, several mirrors are applied in the system (both 7.4 and 10.3 m) to reflect the radiation. We suspect that the slight distortions in the reconstructed image relative to the simulated image for the 10 m stand-off could be due to slight misalignments in the mirrors that deliver the 94 GHz radiation to the imaging array.

According to the detector array configuration and U–V data coverage analysis discussed above, the image of the target with a rectangular shape should be achieved. At this spiral configuration, the spatial resolution range could be calculated, which is 45.3 mm for the smallest baseline and 27.8 mm for the largest baseline [refer to Eq. (3)]. This requires that the size of an imaging target should be between 27 and 45 mm. Also the target shape should match the distribution of U–V points for better results. Figure 7 shows both the simulation and the experimental image of an aluminum foil target in the shape of a rectangle. The size of the target is 20 mm by 40 mm with the detection array located 640 mm from the target.

Clearly, to image extended 2-D images with an arbitrary shape, six baselines corresponding to only four detectors are not sufficient. One needs to increase the number of baselines, for example, by increasing the number of THz detectors in the array. Since only four detectors were available, the number of baselines was increased through rotational synthesis. The numbers of U–V data points (refer to Fig. 3) were increased by rotating the target in 10 deg intervals up to 170 deg. To optimize the U–V coverage, we chose the four receivers to be collinear at the row positions (refer to Fig. 2) before rotation.

Ideally, one would like to rotate the detector array rather than the target. However, rotation of the de-

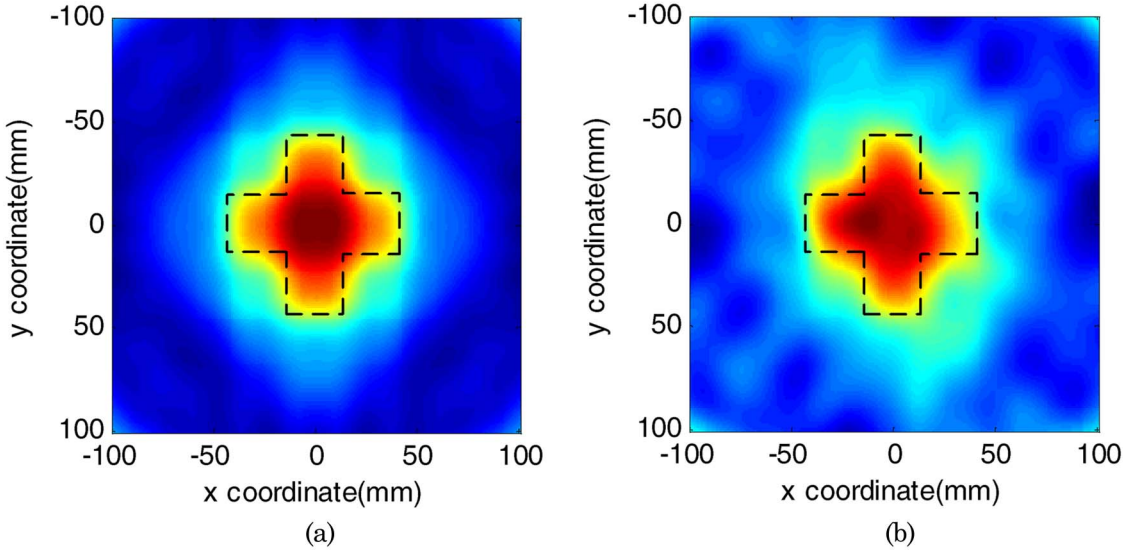

Fig. 8. (Color online) (a) Simulation image of an object shaped as a cross and (b) THz image reconstructed with the experimental data.

tector array would be difficult to implement because of the sensitivity of the detectors to the polarization of the incoming radiation. Rotation of the target should give equivalent results assuming that (a) the target is uniformly illuminated and (b) the rotation axis of the target corresponds to the origin of the detector configuration shown in Fig. 2(a).

Figure 8(a) shows the simulated image of reflected radiation from aluminum foil in the shape of a cross. The object size is 90 mm by 90 mm for the longest dimension in the horizontal and vertical directions, whereas the image distance is 700 mm. Figure 8(b) shows the reconstructed image from experimental data. Although the distortion of the experimental image could be caused by the two conditions mentioned in the previous paragraph, we suspect that the dominant source of distortion is the inherent uncertainty in positioning the rotation axis of the target through the origin of the detector array. Errors in the alignment of the rotation axis will introduce uncertainties in the u and v spatial frequencies and consequently errors in the reconstructed image of Eq. (1).

4. Conclusion

In summary, we have demonstrated a hybrid continuous-wave interferometric imaging system that integrates a millimeter wave source with terahertz photomixing detectors. By use of a high power electronic source (94 GHz Gunn oscillator), this system can image a source at a distance of more than 10 m, demonstrating the promise of interferometric imaging for THz stand-off detection after high power THz sources are developed. Also, by analyzing the amplitude and phase signals for different pairs of detectors and performing the correlation of each baseline, we successfully reconstructed 2-D images of an extended object (aluminum foil) with different shapes. The object is rotated around the fixed axis in 10 deg intervals up to 170 deg to achieve notational synthesis to effectively increase the number of baselines.

The authors gratefully acknowledge the funding assistance of the United States Army Picatinny Arsenal. Program support was provided by Brett Reddingius and Rajen Patel.

References

1. J. F. Federici, B. Schulkin, F. Huang, D. Gary, R. Barat, F. Oliveira, and D. Zimdars, "THz imaging and sensing for security applications-explosives, weapons and drugs," Semicond. Sci. Technol. **20**, S266–S280 (2005).
2. J. F. Federici, D. Gary, R. Barat, and Z.-H. Michalopoulou, "Detection of explosives by terahertz imaging," in *Counter-Terrorism Detection Techniques of Explosives*, J. Yinon, ed. (Elsevier, 2007), p. 323.
3. W. L. Chan, J. Deibel, and D. M. Mittleman, "Imaging with terahertz radiation," Rep. Prog. Phys. **70**, 1325–1379 (2007).
4. B. B. Hu and M. C. Nuss, "Imaging with terahertz waves," Opt. Lett. **20**, 1716–1718 (1995).
5. Q. Wu, T. D. Hewitt, and X.-C. Zhang, "Two-dimensional electro-optic imaging of THz beams," Appl. Phys. Lett. **69**, 1026–1028 (1996).
6. A. R. Thompson, J. M. Moran, and G. W. Swenson, *Interferometry and Synthesis in Radio Astronomy* (Krieger, 1991).
7. K. McClatchey, M. T. Reiten, and R. A. Cheville, "Time resolved synthetic aperture terahertz impulse imaging," Appl. Phys. Lett. **79**, 4485–4487 (2001).
8. A. B. Ruffin, J. Decker, L. Sanchez-Palencia, L. Le Hors, J. F. Whitaker, T. B. Norris, and J. V. Rudd, "Time reversal and object reconstruction with single-cycle pulses," Opt. Lett. **26**, 681–683 (2001).
9. T. D. Dorney, J. L. Johnson, J. Van Rudd, R. G. Baraniuk, W. W. Symes, and D. M. Mittleman, "Terahertz reflection imaging using Kirchhoff migration," Opt. Lett. **26**, 1513–1515 (2001).
10. J. O'Hara and D. Grischkowsky, "Quasi-optic terahertz imaging," Opt. Lett. **26**, 1918–1920 (2001).
11. J. O'Hara and D. Grischkowsky, "Synthetic phased-array terahertz imaging," Opt. Lett. **27**, 1070–1072 (2002).
12. J. O'Hara and D. Grischkowsky, "Quasi-optic synthetic phased-array terahertz imaging," J. Opt. Soc. Am. B **21**, 1178–1191 (2004).
13. T. Löffler, T. May, C. am Weg, A. Alcin, B. Hils, and H. G. Roskos, "Continuous-wave terahertz imaging with a hybrid system," Appl. Phys. Lett. **90**, 091111 (2007).
14. B. Hils, M. D. Thomson, T. Löffler, W. von Spiegel, C. am Weg, H. G. Roskos, P. de Maagt, D. Doyle, and R. D. Geckeler, "Terahertz profilometry at 600 GHz with 0.5 μm depth resolution," Opt. Express **16**, 11289–11293 (2008).
15. J. F. Federici, D. Gary, B. Schulkin, F. Huang, H. Altan, R. Barat, and D. Zimdars, "Terahertz imaging using an interferometric array," Appl. Phys. Lett. **83**, 2477–2479 (2003).
16. A. Bandyopadhyay, A. Stepanov, B. Schulkin, M. Federici, A. Sengupta, D. Gary, J. Federici, R. Barat, Z. H. Michalopoulou, and D. Zimders, "Terahertz interferometric and synthetic aperture imaging," J. Opt. Soc. Am. A **23**, 1168–1178 (2006).
17. K. P. Walsh, B. Schulkin, D. Gary, J. F. Federici, R. Barat, and D. Zimdars, "Terahertz near field interferometric and synthetic aperture imaging," Proc. SPIE **5411**, 9–17 (2004).
18. A. M. Sinyukov, A. Bandyopadhyay, A. Sengupta, R. Barat, D. Gary, Z.-H. Michalopoulou, D. Zimdars, and J. F. Federici, "Terahertz interferometric and synthetic aperture imaging," Int. J. High Speed Electron. Syst. **17**, 431–443 (2007).
19. Z. Liu, K. Su, D. E. Gary, J. F. Federici, R. B. Barat, and Z.-H. Michalopoulou, "Video-rate terahertz interferometric and synthetic aperture imaging," Appl. Opt. **48**, 3788–3795 (2009).